Conductive Polymer and Silicon Composite Secondary Particles for a High Area-loading Negative Electrode

Shidi Xun[a], Bin Xiang[b], Andrew Minor[b], Vince Battaglia[a], Gao Liu[a,] *

[a]Environmental Energy Technologies Division

Lawrence Berkeley National Laboratory

1 Cyclotron Rd.

Berkeley, CA 94720

USA

[b]National Center for Electron Microscopy

Lawrence Berkeley National Laboratory

&

Department of Materials Science & Engineering

University of California

Berkeley, CA 94720

USA

*Corresponding author: gliu@lbl.gov

Abstract

A conductive polymer and silicon nanoparticles were used to form elastic and porous micron-sized composite secondary particles using spray precipitation method. These composite secondary particles are used to fabricate a lithium-ion anode electrode. Although the Si volume changes during charge and discharge process, the composite secondary particles retain their size during these processes, to maintain a stable electrode microstructure. This dimension stability leads to improved electrode cycling stability and enhanced rate performance.

Introduction

Silicon (Si) material has high lithium-ion alloy capacity of 4,200 mAh/g.[1, 2] At least a 3,580 mAh/g reversible lithium-ion capacity can be achieved via electrochemical process under the similar conditions of reversible lithiation and delithiation of graphite materials,[3, 4] which has only 372 mAh/g of lithium-ion capacity.[5] The high capacity makes Si an attractive material for the lithium-ion negative electrode application, to further improve the energy density of rechargeable lithium-ion batteries.

However, the high lithium-ion capacity comes with a proportional Si volume change, up to 300% volume expansion, from pure Si to $Li_{4.4}Si$.[3, 4, 6] In a conventional lithium-ion electrode, such as a graphite or lithium cobalt oxide ($LiCoO_2$)-based electrode, lithium-ion storage particles are normally 1 to10 micrometer (μm)-sized particles.[7] This large volume change of Si induces high stress within the micron sized Si particles, leading to mechanical breakdown of the particles.[8-12] Nanosizing the Si particles can significantly reduce crack formation, resulting in better material integrity during the lithiation/delithiation process.[13] Particle size preferably should be below 150 nm to significantly reduce crack formation.[8, 14]

To make robust electrical connections to the nano-Si particles, a conductive polymer binder was developed. The binder combines adhesion with electrical conduction to provide molecular-level electronic connections between the Si nanoparticles and the conductive polymer matrix.[15] This approach has significantly enhanced the cycling

stability of the Si electrode. However, the large volume change of the Si nanoparticle during cycling has caused binder migration in the electrode, leading to reduced pore sizes after just a few cycles. The gradual reduction of pore size seals off the ion-transport channels in the porous electrode, resulting in capacity fade. This failure mechanism is more pronounced as the electrode area loading of the active material and the thickness of electrode increases.[16] A study based on thickness of the Si electrode has shown that area-specific capacity is inversely related to the cycling performance (**Supplemental Figure 1**). As the Si area loading in the electrode gets higher, the cycling performance decays significantly. This phenomenon is observed in all the Si-based and other active materials based electrodes, but more pronounced in Si-based electrodes. Both the ion-transport distance and tortuosity of the pores in the composite secondary electrode increase as the electrode's thickness increases. Therefore, lithium-ion diffusion is impeded with the increase of electrode thickness. Therefore, it is important to isolate the impact of Si volume change within micron-size domains, so as not to affect the overall electrode micro-structures. This is achieved by the following steps, as shown in **Figure 1**: First, form micron-size Si nanoparticle/conductive polymer composite secondary particles; then build in porosity in the composite secondary particles, so the Si nanoparticle volume change during lithiation can be accommodated within the composite secondary particles (i.e., there is no volume change in the composite secondary particle level) (**Figure 1a**). Finally, assemble the composite secondary particles into a regular porous electrode, with pores among the composite secondary particles (**Figure 1b**).

Experimental

Silicon nanoparticles were purchased from Sigma-Aldrich and used without further purification. The particle size defined by the company is less than 100 nm. Transmission electron microscopy analysis shows a bimodal particle size distribution at the 50 nm and 10 nm diameter ranges. The conductive polymer binder is poly(9,9-dioctylfluorene-co-fluorenone-co-methylbenzoic ester) material, which was designed by the authors and synthesized by Battelle Memorial Institute. The conductive polymer binder has a molecular weight of 28,000 dalton and a polydispersity of 4.0. Battery-grade acetylene black with an average particle size of 40 nm, a specific surface area of 60.4 square meters per gram (m^2/g), and a material density of 1.95 grams per cubic centimeter (g/cm^3) was acquired from Denka Singapore Private Ltd. Chlorobenzene and methanol were purchased from Aldrich Chemical Co. The 1 M $LiPF_6$ in ethylene carbonate and fluorinated ethylene carbonate (7:3 w/w) electrolyte was purchased from Novolyte Technologies of BASF.

The Si/conductive polymer slurry and process for making the planar electrode were previously reported.[15] The slurry making process and the weight ratio of conductive polymer to Si in the composite are described in detail in Supporting Information of reference [15]. The Si/conductive polymer composite secondary particle was made with the sonication spray-precipitation process. The Si/conductive polymer slurry was fed by syringe pump at the rate of 0.1 liters per hour (L/h). The power of the ultrasonic atomizer

was set as 50%. The nanoporous spheres were sprayed to a large amount of methanol. Methanol is a non-solvent of the conductive polymer. After the particles were precipitated, methanol was decanted. The proper amount of carboxylmethyl cellulose binder and carbon black aqueous solution was added. Then the slurry was stirred for one hour with a magnetic bar. The composition of the electrode is 10% carboxymethyl cellulose (CMC), 10% acetylene black, and 80% Si composite secondary sphere. The uniform slurry was cast on copper foil. The thickness of electrodes was controlled by doctor blade gap to achieve the desired area capacity loading. The cross-section of composite secondary particles was acquired with Focused Ion Beam (FIB) milling. The cross section of electrodes was acquired by freezing the electrode laminate in liquid nitrogen and folding the electrode laminate to break and expose the cross section. The SEM imaging was performed on the composite secondary particles surface and cross section, and electrode surface and cross section. The FIB and SEM process were reported previously.[17] Lithium metal counter electrode coin cells were fabricated. The cell fabrication and electrochemical testing were performed according to the literature procedures.[7, 15]

Results & Discussion

The composite secondary particle dimension and design are crucial for the success of this approach. The dimension of the composite secondary particle has to allow the facile lithium-ion transport. This is determined experimentally by fabricating different thicknesses of planar electrodes and conducting rate and cycling tests of those electrodes.

The planar Si electrode was fabricated by coating of the slurry of conductive polymer and Si nanoparticle directly on to Cu current collector, and drying at elevated temperature to form a electrode laminate. The capacity decay of the planar electrode at different thickness and Si loading is used to determine the critical dimension of this composite secondary system. The cycling performance is reported based on a C/10 rate current density, which consumer electronics use for a high-energy battery system. The performance varies according to the C-rate. The planar laminate electrodes with thickness less than 10 μm show stable cycling performance (**Supplemental Figure 1a**). The planar electrode only allows lithium diffusion from the top to the bottom of the electrode. Therefore, the critical diameter for a spherical composite secondary particle is less than 20 μm, because the lithium-ion can diffuse from any direction of the spherical surface. The capacity fades quickly if the engineered composite secondary particle diameter is larger than the critical dimensions, but if the composite secondary particles are too small, it will lose the benefit of accommodating volume change of the primary Si nanoparticles.

A sonication spray-precipitation method was used to generate spherical composite secondary particles (**Supplemental Figure 2**). Controlled strength of ultrasound dispersion was used during the spray of Si/conductive polymer composite secondary slurry into a non-solvent of the conductive polymer to produce a spherical precipitate. By controlling the slurry solvent content and sonication strength, the average size and porosity of the composite secondary particle precipitated can be controlled. The porosity within the composite secondary particles can provide dimensional stability in the composite secondary particle level, while the primary nanoparticles can freely expand

and contract. This dimensional stability of the composite secondary particles maintains porosity among the composite secondary particles, to ensure stable ion-transport properties in the electrode level. This will allow the fabrication of higher area loading of Si electrode.

Spherical composite secondary particles were fabricated, as shown in **Figure 2**. An average particle size of 10 μm in diameter was achieved, as seen in the scanning electron microscope (SEM) image of the particles collected after the spray-precipitation from the methanol non-solvent (**Figure 2a,b**). The initial droplet size from the spray nozzle is controlled by the ultrasonic power at the nozzle. The smallest droplet diameter can be achieved is around 20 μm based on the manufacturer's configuration. Further reduction of composite secondary particle size was achieved by increasing the chlorobenzene solvent content of the slurry. The dried composite secondary particles, ranging from 2 μm diameter to 20 μm diameter, were made when controlled at the smallest spray droplet of 20 μm diameter. The higher the solvent content in the slurry, the further size reduction there is after the droplets precipitate into the non-solvent. When the slurry droplets are sprayed into the non-solvent, the migration of slurry solvent from the droplets to the none-solvent starts from the surface of the droplets. The surface polymer solidifies first. The particle size will be partially fixed before the center slurry solvent all migrates out of the spheres. A higher solvent amount in the slurry tends to produce smaller particles with higher porosity. In large particles, void space in the middle of the particles can be detected. The particle size distribution is large using this method.

Focused Ion Beam (FIB) was used to mill out the cross-section of the composite secondary particles. The cross-section SEM images show the extended porosity in the composite secondary particles (**Figure 2c,d** and **Supplementary Figure 3**), which allows the Si primary nanoparticle to expand. The distribution of a conductive polymer binder and Si n the composite secondary particle is very uniform, as show in the Energy-dispersive X-ray spectroscopy (EDS) mapping image of the elemental Si, carbon (C), and oxygen (O) in **Figure 2e-h** and **Supplementary Figure 3**. This composite secondary design has advantages over a Si nanoparticle in a carbon matrix made by a high-temperature carbonation process.[18-22] The Si nanoparticles/conductive polymer composite secondary particles have high internal porosity and more elastic than carbon matrix, critical for materials with huge volume change during cycling, such as Si or tin (Sn). The conductive polymer binder is also covalently adhesive to the SiO_2 surface to maintain mechanical connectivity during the expansion and contraction of nano-Si primary particles.[15, 23] Thus, the integrity of secondary particles can be retained during cycling.

The different Si loading electrodes based on the composite secondary particles were fabricated and tested in a coin cell with lithium metal as a counter electrode and reported in **Figure 3**. The capacity retention during the initial cyclings of the electrodes shows the improved stability. For the planar electrode design, the delithiation capacity drops to 60% of its original capacity, at 1.8 mAh per square centimeter (cm^2) loading after 28 cycles (**Supplemental Figure 1a**); whereas, for the electrode design based on composite secondary particles, the capacity decay is minimum (**Figure 3a**). The planar electrodes have no cyclable capacity at 4 mAh/cm^2 loading; whereas, the electrode made with

composite secondary particles cycles well in this loading range. The Si utilizations are above 2500 mAh/g in all four different loadings (**Figure 3b**). This is similar to the best Si utilization of the low loading planar electrodes. The high current density delithiation is also improved as lithium-ion transport improves within the composite secondary particle based electrode. There is less than 10% capacity decrease from C/10 current density to 5C delithiation (**Figure 3c, Supplemental Figure 4a,b**). However, the planar electrode has over 25% decreases at similar loading (**Supplemental Figure 4c**).

To further demonstrate the reasons behind the performance enhancement of this approach, the electrode surfaces and cross-sections before and after cycling were examined by SEM (**Figure 4**). The electrode was made of composite secondary particles in the size rang of a few to 20μm diameter made by the spray precipitation method. The particle size distribution is large and the large particles tend to be hollow. The large secondary particles tend to deform during cycling due to the volume changes toward the inside of the hollow space. The secondary composite particles create not only high porosity but also bigger pore sizes among them in the electrode to facilitation Li-ion transport. Although the fresh planar electrodes have higher porosity, the pores are much smaller. After only one cycle, mot of the fine pore channels are sealed off by the movement of the Si particles (**Supplemental Figure 1b,c**). In the composite secondary particle based electrode, although some of the large secondary composite particles deforms after cycling, the large pore channels among the secondary composite particles can be largely maintained after cycling. The porosity of the fresh electrode made with composite secondary particles can be observed both on the surface and in the laminate

cross section. The cycling of the electrode does not significantly alter the large pores among the composite secondary particles. These stable and large pores hold electrolyte during cycling, facilitating ion transport in the high-loading electrode.

Conclusions

A high-performance composite secondary electrode for a large-volume-change active materials can be achieved through design of the both materials and the electrode. The design principles include the following:

- Si nanoparticles are used for lithium-ion storage and mitigate material-level breakdown during lithiation and delithiation.
- The Si nanoparticles and a conductive polymer binder are used to form composite secondary particles, which have the porosity to accommodate volume change of the Si nanoparticle.
- The dimension-stable composite secondary particles are used to form the electrode.

A proof-of-concept facile approach was demonstrated using a sonication spray and precipitation method to prepare Si nanoparticles and polymer composite secondary spherical particles in the range of 10 μm in diameter. This-electrode using the composite secondary particles has loading above 3 mAh/cm^2, and has demonstrated significantly improved cycling stability over the regular planar electrode design.

Acknowledgements

This work was funded by the Assistant Secretary for Energy Efficiency, Office of Vehicle Technologies of the U.S. Department of Energy (U.S. DOE) under contract no. DE-AC02-05CH11231 under the Batteries for Advanced Transportation Technologies (BATT) Program, and by the University of California, Office of the President, through the University of California Discovery Grant. Focused Ion Beam (FIB) and electron microscopy experiments were performed at the National Center for Electron Microscopy, funded by the Office of Science, Office of Basic Energy Sciences, of the U.S. DOE under Contract No. DE-AC02-05CH11231.

References

1. D. Larcher, S. Beattie, M. Morcrette, K. Edstroem, J. C. Jumas and J. M. Tarascon, *J. Mater. Chem.*, 2007, **17**, 3759-3772.
2. B. A. Boukamp, G. C. Lesh and R. A. Huggins, *Journal of the Electrochemical Society*, 1981, **128**, 725-729.
3. J. Li and J. R. Dahn, *J. Electrochem. Soc.*, 2007, **154**, A156-A161.
4. M. N. Obrovac and L. J. Krause, *Journal of the Electrochemical Society*, 2007, **154**, A103-A108.
5. T. Ohzuku, Y. Iwakoshi and K. Sawai, *J. Electrochem. Soc.*, 1993, **140**, 2490-2498.
6. J. Li, R. B. Lewis and J. R. Dahn, *Electrochemical and Solid State Letters*, 2007, **10**, A17-A20.
7. G. Liu, H. Zheng, X. Song and V. S. Battaglia, *Journal of the Electrochemical Society*, 2012, **159**, A214-A221.
8. M. J. Chon, V. A. Sethuraman, A. McCormick, V. Srinivasan and P. R. Guduru, *Physical Review Letters*, 2011, **107**.
9. A. F. Bower, P. R. Guduru and V. A. Sethuraman, *Journal of the Mechanics and Physics of Solids*, 2011, **59**, 804-828.
10. J. Christensen and J. Newman, *Journal of Solid State Electrochemistry*, 2006, **10**, 293-319.
11. S. W. Lee, M. T. McDowell, J. W. Choi and Y. Cui, *Nano Letters*, 2011, **11**, 3034-3039.
12. S. W. Lee, M. T. McDowell, L. A. Berla, W. D. Nix and Y. Cui, *Proceedings of the National Academy of Sciences of the United States of America*, 2012, **109**, 4080-4085.
13. C. K. Chan, H. Peng, G. Liu, K. McIlwrath, X. F. Zhang, R. A. Huggins and Y. Cui, *Nature Nanotechnology*, 2008, **3**, 31-35.
14. X. H. Liu, L. Zhong, S. Huang, S. X. Mao, T. Zhu and J. Y. Huang, *Acs Nano*, 2012, **6**, 1522-1531.
15. G. Liu, S. Xun, N. Vukmirovic, X. Song, P. Olalde-Velasco, H. Zheng, V. S. Battaglia, L. Wang and W. Yang, *Advanced Materials*, 2011, **23**, 4679-+.
16. S. Renganathan, G. Sikha, S. Santhanagopalan and R. E. White, *Journal of the Electrochemical Society*, 2010, **157**, A155-A163.
17. S. Kim, M. J. Park, N. P. Balsara, G. Liu and A. M. Minor, *Ultramicroscopy*, 2011, **111**, 191-199.
18. J. Liu, T. E. Conry, X. Song, M. M. Doeff and T. J. Richardson, *Energy & Environmental Science*, 2011, **4**, 885-888.
19. J. Liu, T. E. Conry, X. Song, L. Yang, M. M. Doeff and T. J. Richardson, *Journal of Materials Chemistry*, 2011, **21**, 9984-9987.
20. S. Gurmen and B. Ebin, *Journal of Alloys and Compounds*, 2010, **492**, 585-589.
21. S. Gurmen, B. Ebin, S. Stopic and B. Friedrich, *Journal of Alloys and Compounds*, 2009, **480**, 529-533.
22. S. Gurmen, A. Guven, B. Ebin, S. Stopic and B. Friedrich, *Journal of Alloys and Compounds*, 2009, **481**, 600-604.

23. N. S. Hochgatterer, M. R. Schweiger, S. Koller, P. R. Raimann, T. Woehrle, C. Wurm and M. Winter, *Electrochemical and Solid State Letters*, 2008, **11**, A76-A80.

Figure captions

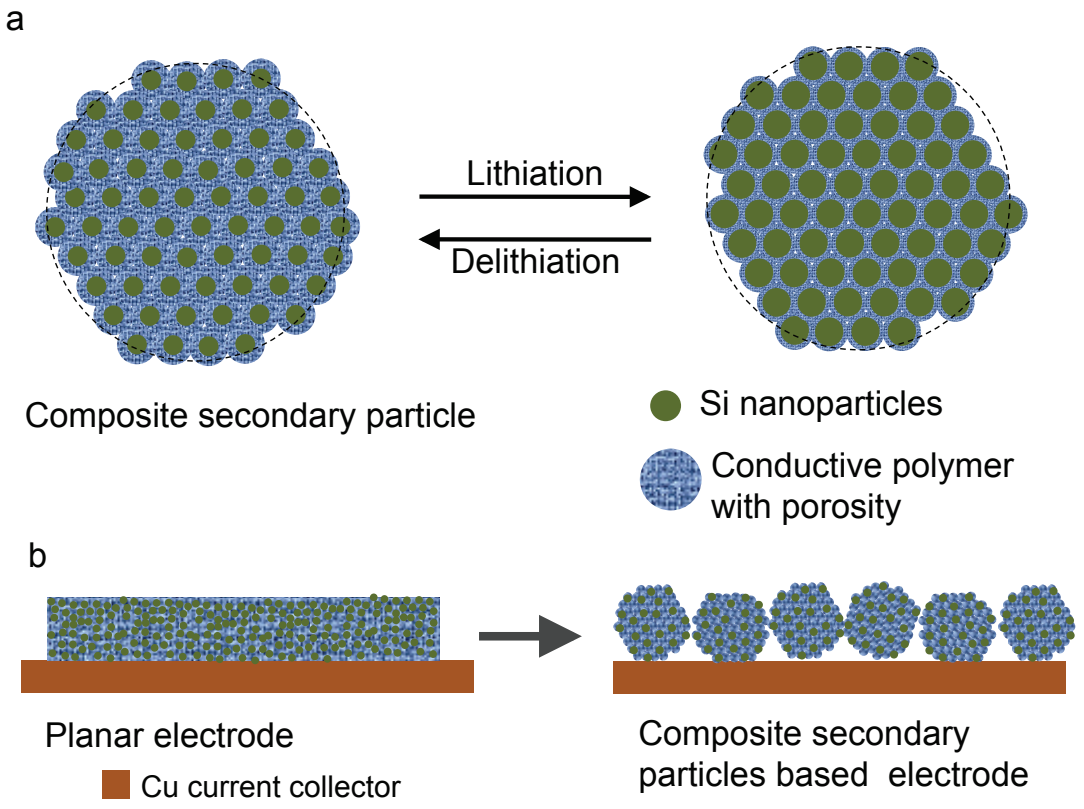

Figure 1. Schematic of the materials and electrode design based on Si/conductive polymer composite secondary particles. **a**. Composite secondary particles have a stable dimension during Si lithiation and delithiation. The dotted lines are for visual guidance. **b**. A planar electrode made with a conductive polymer binder and Si nanoparticles vs. an electrode made with composite secondary particles. There are larger pores between the composite secondary particles.

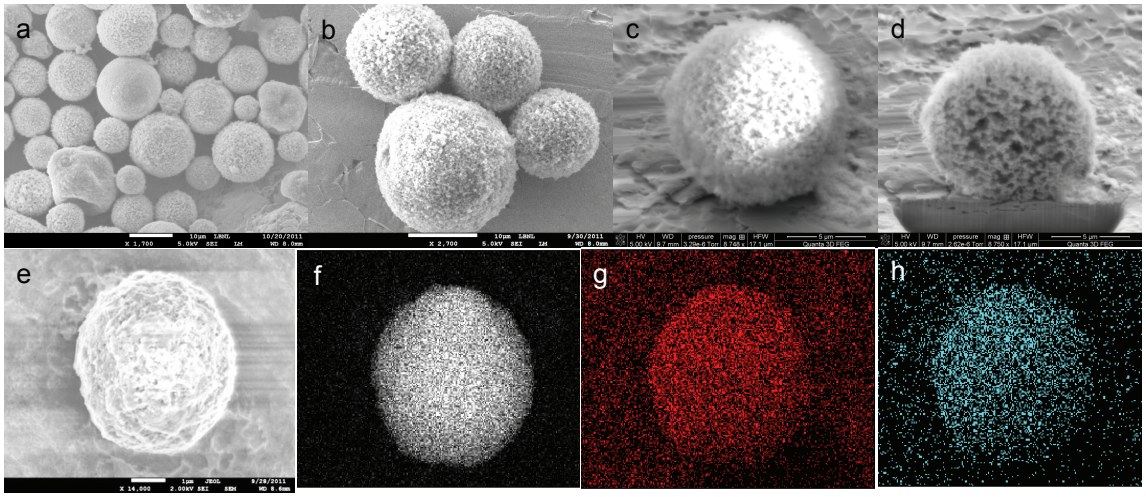

Figure 2. SEM images of the Si/conductive polymer composite secondary particles. **a**,**b.** Collected after spray-precipitation at different magnifications. **c**,**d.** A single particle and its cross-section image. **e-h.** A single particle and its EDS mapping image of silicon, oxygen, and carbon

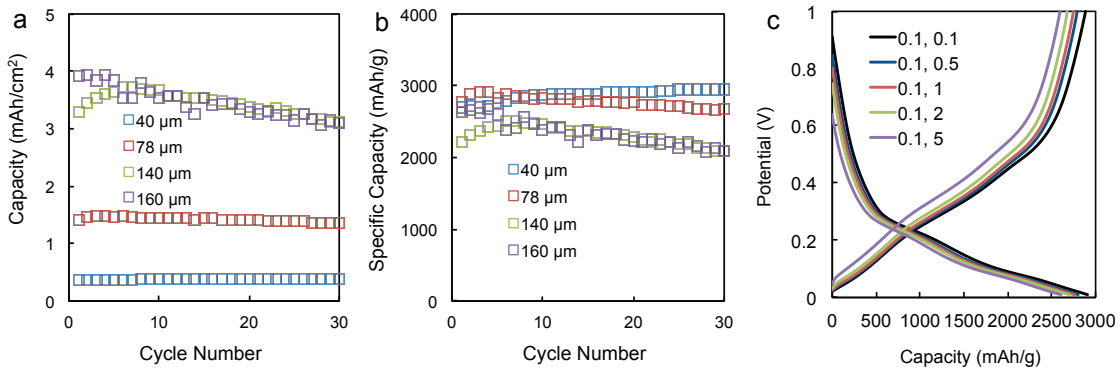

Figure 3. Cycling and rate performance of the electrode made with a Si/conductive polymer binder composite secondary particles. **a**. Significantly improved loading and cycling stability. **b.** The gravimetric specific capacities based on Si contents in the electrode. **c.** Significantly improved rate performance (C/10 rate lithiation and variable rate delithiation).

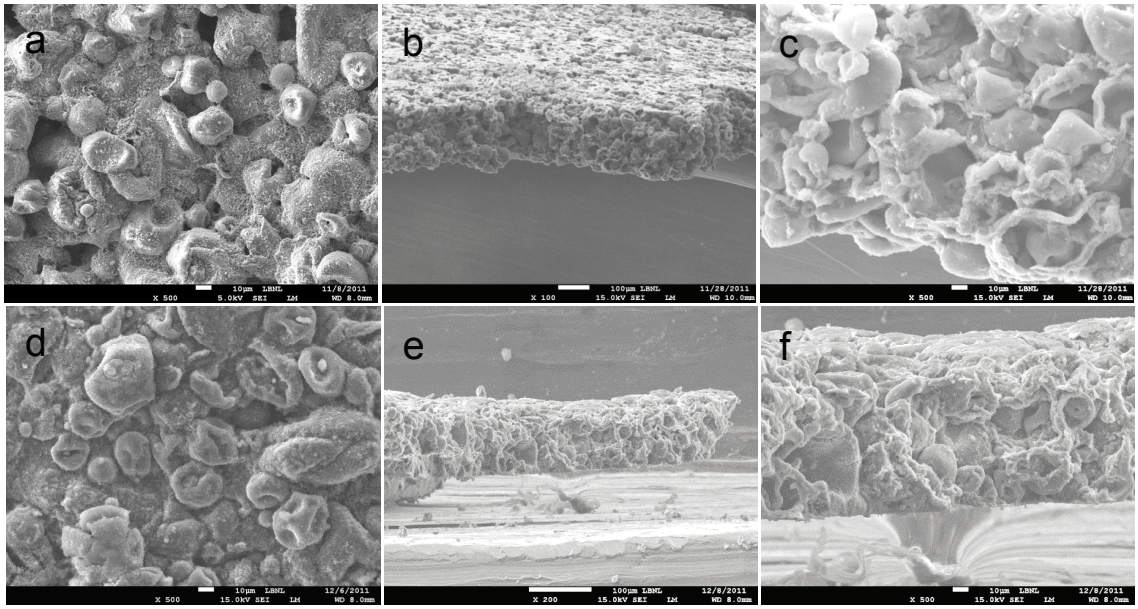

Figure 4. The electrodes made with Si/conductive polymer composite secondary particles. **a.** SEM surface image of the fresh electrode shows porosity. **b.** Cross section of the fresh electrode. **c.** Higher resolution cross-section of the fresh electrode shows particle-to-particle porosity. **d.** SEM surface image of the cycled electrode shows porosity. **e**. Cross section of the cycled electrode. **f.** Higher-resolution cross section of the electrode shows that particle-to-particle porosity remains after cycling.